Empirical mode decomposition based background removal and de-noising in polarization interference imaging spectrometer

Chunmin Zhang,[1,2,*] Wenyi Ren,[1,2,3] Tingkui Mu,[1,2] Lili Fu[1,3] and Chenling Jia[1,2]

[1]*School of science, Xi'an Jiaotong University, Xi'an 710049, China*
[2]*Non-equilibrium Condensed Matter and Quantum Engineering Laboratory, the Key Laboratory of the Ministry of Education, Xi'an 710049, China*
[3]*Xi'an Institute of Optics and Precision Mechanics, Chinese Academy of Science (CAS), Xi'an 710119, China*
[*]*zcm@mail.xjtu.edu.cn*

Abstract: Based on empirical mode decomposition (EMD), the background removal and de-noising procedures of the data taken by polarization interference imaging interferometer (PIIS) are implemented. Through numerical simulation, it is discovered that the data processing methods are effective. The assumption that the noise mostly exists in the first intrinsic mode function is verified, and the parameters in the EMD thresholding de-noising methods is determined. In comparison, the wavelet and windowed Fourier transform based thresholding de-noising methods are introduced. The de-noised results are evaluated by the SNR, spectral resolution and peak value of the de-noised spectrums. All the methods are used to suppress the effect from the Gaussian and Poisson noise. The de-noising efficiency is higher for the spectrum contaminated by Gaussian noise. The interferogram obtained by the PIIS is processed by the proposed methods. Both the interferogram without background and noise free spectrum are obtained effectively. The adaptive and robust EMD based methods are effective to the background removal and de-noising in PIIS.

OCIS codes: (070.0070) Fourier optics and signal processing; (300.0300) Spectroscopy.

References and links

1. C. Zhang, X. Bin, and B. Zhao, "Static polarization interference imaging spectrometer (SPIIS)," Proc. SPIE **4087**, 957–961 (2000).
2. L. Wu, C. Zhang, and B. Zhao, "Analysis of the lateral displacement and optical path difference in Wide-field-of –view polarization interference imaging spectrometer," Opt. Commun. **273**(1), 67–73 (2007).
3. X. Jian, C. Zhang, L. Zhang, and B. Zhao, "The data processing of the temporarily and spatially mixed modulated polarization interference imaging spectrometer," Opt. Express **18**(6), 5674–5680 (2010).
4. C. Zhang and X. Jian, "Wide-spectrum reconstruction method for a birefringence interference imaging spectrometer," Opt. Lett. **35**(3), 366–368 (2010).
5. W. Ren, C. Zhang, T. Mu, and H. Dai, "Spectrum reconstruction based on the constrained optimal linear inverse methods," Opt. Lett. **37**(13), 2580–2582 (2012).
6. T. Mu, C. Zhang, W. Ren, and C. Jia, "Static polarization-difference interference imaging spectrometer," Opt. Lett. **37**(17), 3507–3509 (2012).
7. T. Mu, C. Zhang, C. Jia, and W. Ren, "Static hyperspectral imaging polarimeter for full linear Stokes parameters," Opt. Express **20**(16), 18194–18201 (2012).
8. N. E. Huang, Z. Shen, S. R. Long, M. C. Wu, H. H. Shih, Q. Zheng, N.-C. Yen, C. C. Tung, and H. H. Liu, "The empirical mode decomposition and the Hilbert spectrum for nonlinear and non-stationary time series analysis," Proc. R. Soc. Lond. A **454**(1971), 903–995 (1998).
9. Z. Wu and N. E. Huang, "A study of the characteristcs of white noise using the Empirical Mode Decomposition method," Proc. R. Soc. Lond. A **460**(2046), 1597–1611 (2004).
10. N. E. Huang, Z. Shen, and S. R. Long, "A new view of nonlinear water waves: The Hilbert spectrum," Annu. Rev. Fluid Mech. **31**(1), 417–457 (1999).
11. P. Flandrin, G. Rilling, and P. Gonçalves, "Empirical mode decomposition as a filter bank," IEEE Signal Process. Lett. **11**(2), 112–114 (2004).

#179604 - $15.00 USD Received 9 Nov 2012; revised 28 Dec 2012; accepted 12 Jan 2013; published 28 Jan 2013

12. P. D. Spanos, A. Giaralis, and N. P. Politis, "Time-frequency representation of earthquake accelerograms and inelastic structural response records using the adaptive chirplet decomposition and empirical mode decomposition," Soil. Dyn. Earthquake Eng. **27**(7), 675–689 (2007).
13. A. O. Boudraa and J. C. Cexus, "EMD-based signal filtering," IEEE Trans. Instrum. Meas. **56**(6), 2196–2202 (2007).
14. A. Moghtaderi, P. Borgnat, and P. Flandrin, "Trend filtering: empirical mode decompositions Versus l1 and Hodrick-Prescott," Adv. Adapt. Data Anal. **3**, 41–61 (2011).
15. H. Liang, Z. Lin, and R. W. McCallum, "Artifact reduction in electrogastrogram based on empirical mode decomposition method," Med. Biol. Eng. Comput. **38**(1), 35–41 (2000).
16. H. Liang, Q. H. Lin, and J. D. Z. Chen, "Application of the empirical mode decomposition to the analysis of esophageal manometric data in gastroesophageal reflux disease," IEEE Trans. Biomed. Eng. **52**(10), 1692–1701 (2005).
17. M. Blanco-Velasco, B. Weng, and K. E. Barner, "ECG signal de-noising and baseline wander correction based on the empirical mode decomposition," Comput. Biol. Med. **38**(1), 1–13 (2008).
18. Q. Gao, C. Duan, H. Fan, and Q. Meng, "Rotating machine fault diagnosis using empirical mode decomposition," Mech. Syst. Signal Process. **22**(5), 1072–1081 (2008).
19. R. J. Bell, *Introductory Fourier Transform Spectroscopy* (Academic Press & London, 1972), Chap. 3.
20. A. O. Boudraa, J. C. Cexus, and Z. Saidi, "EMD-based signal noise reduction," Int. J. Signal Process. **1**, 33–37 (2004).
21. L. Donoho, "De-noising by soft-thresholding," IEEE Trans. Inf. Theory **41**(3), 613–627 (1995).
22. Q. Kemao, "A simple phase unwrapping approach based on filtering by windowed Fourier transform: a note on the threshold selection," Opt. Laser Technol. **40**(8), 1091–1098 (2008).

1. Introduction

1.1 Polarization interference imaging spectrometer

In 2000, Zhang *et al.* [1] proposed a polarization interference imaging spectrometer (PIIS) based on the Savart polariscope. Firstly, an incident beam is split into two beams by the Savart polariscope and their polarization directions are identical when they passed through an analyzer. Finally, the two beams interfere on the focal plane of the imaging lens [2]. Based on the data acquisition principle of a windowing spectrometer, the original data including the interferogram and image of object is obtained. According to the data processing methods used in a PIIS, the information (including image, spectrum and polarization) can be retrieved [3–7]. A row of the contaminated interferogram, with background and noise, acquired by the PIIS, can be expressed as [5]

$$I_c(x) = \sum_{j=1}^{j=N} B_j \cos[2\pi\sigma_j \Delta_j(x)] + b(x) + n(x), \qquad (1)$$

where B_j and Δ_j are the spectrum radiation and optical path difference as functions of the wavenumber σ_j, respectively. $b(x)$ is the background which is a slow varying function of location x, and $n(x)$ is the additive noise. During signal processing, background also is named as trend. Usually, the image information of objects can be obtained from the background of the image data taken by the PIIS.

1.2. Empirical mode decomposition

Empirical mode decomposition (EMD) has been recently pioneered by Huang et al. (1998) for adaptively decomposing signals into a sum of amplitude modulation frequency modulation (AM-FM) components, which consist of naturally "intrinsic" building blocks that describe the complicated waveform [8]. Contrary to previous decomposition methods such as Fourier transform, discrete cosine transform and wavelet transform etc., EMD is empirical, intuitive, direct, adaptive, and it does not require any predetermined basis functions [8–11]. The decomposition, based on the principle of local scale separation, is designed to seek the different intrinsic modes of oscillations in any data. An intrinsic mode of oscillation is called as an intrinsic mode function (IMF) when it satisfies two criteria [8]: (*i*) in the whole data set, the numbers of extrema and zero-crossings must either equal or differ at most by one and (*ii*) at any

#179604 - $15.00 USD Received 9 Nov 2012; revised 28 Dec 2012; accepted 12 Jan 2013; published 28 Jan 2013

point, the mean value of the envelopes defined by the local maxima and minima is zero. For any one-dimensional discrete signal, EMD is expressed as

$$s(x) = \sum_{i=1}^{i=K} c_i(x) + r(x), \tag{2}$$

where c_i is the i^{th} IMF of the signal s, and r is the residual trend (a low-order polynomial component). If we interpret the EMD as a timescale analysis method, lower and higher order IMFs correspond to the fine and coarse scales, respectively.

EMD has been successfully employed in various applications [12–18]. However, there are no studies that apply the EMD based data processing of the PIIS or Fourier transform spectrometer (FTS). In this paper, a partial reconstruction method is proposed to remove the background of the obtained interferogram, and another to suppress the effect from the noise in the spectrum. The feasibility of the proposed methods is verified through numerical simulation.

2. The EMD based data processing in the PIIS

2.1 Background removal

Based on EMD, the interferogram $I_c(x)$ obtained in Eq. (1) is decomposed into K IMFs,

$$I_c(x) = \sum_{i=1}^{i=K} c_i(x) + r(x). \tag{3}$$

Generally, lower order IMFs capture high frequency modes while higher order IMFs typically represent low frequency modes. The background can be partially reconstructed with the higher order IMFs and residual. The reconstruction method is formulized as

$$\begin{aligned} I_p(x) &= \sum_{i=D+1}^{i=K} c_i(x), \\ b_e(x) &= \sum_{i=D+1}^{i=K} c_i(x) + r(x), \end{aligned} \tag{4}$$

where $I_p(x)$, $b_e(x)$ and D are the interferogram without background, estimated background and the interferogram's largest IMF index without background contamination. Each of the IMFs is zero mean. A rule of thumb for choosing D is implemented by the following steps:

(i) Calculate the absolute value of the sum of samples of the signal reconstructed using the first d IMFs by

$$S(d) = \left| \sum_{i=1}^{i=d} \sum_{x} c_i(x) \right|, d = 1, \cdots, K. \tag{5}$$

(ii) Pick out the minimal one of $S(d)$ which is larger than zero significantly. The index of the picked $S(d)$ is estimated as $D+1$.

Generally, the background is estimated as a constant $\frac{1}{2} I(\Delta = 0)$ [19]. Comparing with the traditional background estimation method, the EMD based methods can provide a slowly varying background but not a constant.

2. 2 De-noising

According to Fourier transform spectroscopy [19], the contaminated spectrum B_c can be obtained via the Fourier transform of contaminated interferogram I_c. Via EMD, B_c can be decomposed into M IMFs and residual as

$$B_c(\sigma) = \sum_{i=1}^{i=M} B_{ic}(\sigma) + B_{rc}(\sigma), \tag{6}$$

#179604 - $15.00 USD Received 9 Nov 2012; revised 28 Dec 2012; accepted 12 Jan 2013; published 28 Jan 2013

where B_{ic} and B_{rc}, respectively, are the i^{th} mode and the residual mode.

The noise traditionally is characterized by high frequency. Thus, instead of de-noising to each IMF, one can de-noise to a given number of IMFs. A generalized reconstruction of the noise free spectrum is given by

$$B(\sigma) = \sum_{i=K_1}^{i=K_2} B_i(\sigma) + \sum_{i=K_2+1}^{i=M} B_{ic}(\sigma) + B_{rc}(\sigma), \tag{7}$$

where, $B(\sigma)$ and $B_i(\sigma)$, respectively, are the noise free spectrum and i^{th} noise free IMF; the parameters K_1 and K_2 gives us flexibility on the exclusion of the noisy low order IMFs. Indeed, as in wavelet analysis, the energy of the noise will often be concentrated on the high frequency temporal modes (first IMFs) and decreases towards the coarser ones (last IMFs). It also turns out that the first IMF carries the greatest noise power [20]. Hence, the noise free spectrum B can be reconstructed as

$$B(\sigma) = B_1(\sigma) + \sum_{i=2}^{i=M} B_{ic}(\sigma) + B_{rc}(\sigma), \tag{8}$$

Inspired by wavelet thresholding [21], B_1 is obtained by

$$B_1(\sigma) = \mathrm{sgn}[B_{1c}(\sigma)] \max(|B_{1c}(\sigma)| - \tau_1, 0), \tag{9}$$

where sgn[ ] is the sign function, and τ_1 is the threshold of B_{1c}. According to the strategy used in the soft-threshold filtering based on wavelet described by Donoho [21], τ_1 is given by

$$\begin{aligned} &\tau_1 = \gamma \kappa_1 \sqrt{2\log(T)}, \\ &\kappa_1 = \mathrm{MAD}_1 / 0.6745, \\ &\mathrm{MAD}_1 = \mathrm{Median}\{|B_{1c}(\sigma) - \mathrm{Median}\{B_{1c}(\sigma)\}|\}, \end{aligned} \tag{10}$$

where γ is a constant, T is the length of the contaminated spectrum, κ_1 is the estimation of the noise level of $B_{1c}(\sigma)$, and MAD_1 is the absolute median deviation of $B_{1c}(\sigma)$.

3. Simulation

In order to verify the feasibility of the methods proposed in Sec. 2, a simulation was performed. As shown in Fig. 1, a noise free interferogram I_o was simulated based on the principle of the PIIS [1–7]. A slowly varying function as the background was added into I_o and then it was contaminated by an assumed Gaussian noise. The contaminated interferogram I_c with SNR of 5dB is shown in Fig. 1.

#179604 - $15.00 USD Received 9 Nov 2012; revised 28 Dec 2012; accepted 12 Jan 2013; published 28 Jan 2013

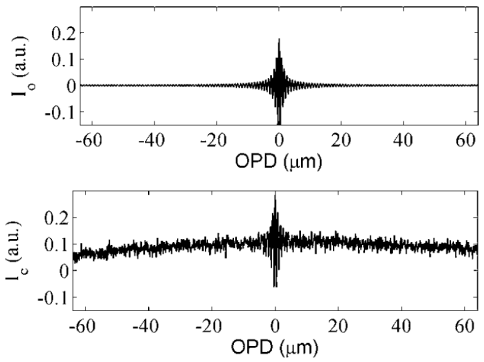

Fig. 1. The simulated noise free interferogram (the up) and contaminated interferogram (the down).

3.1 Background removal

As shown in Fig. 2, the contaminated interferogram was decomposed into 16 IMFs (including the residual mode). Note that, as we had mentioned previously, the varying frequencies of the IMF with small indices are higher than that with large indices. According to the obtained IMFs, the background of the contaminated interferogram can be eliminated by the methods proposed in section 2.1. The relationship between them is described by the curve in Fig. 3(a). It is discovered that S is significantly larger than 0 while d = 11. Thereby, D is 10. The summation of the IMFs 1 to 10 is estimated as the interferogram without background. The summation of the IMFs 11 to 15 and residual is the estimated background. The estimated and assumed backgrounds are both depicted in Fig. 3(b) and they are similar to each other. The background is effectively estimated by the modified method described in Eq. (4).

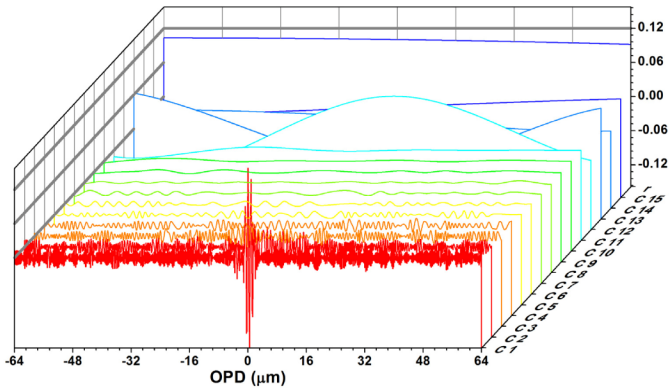

Fig. 2. The simulated noise free interferogram is decomposed into 16 IMFs (including the residual mode).

#179604 - $15.00 USD Received 9 Nov 2012; revised 28 Dec 2012; accepted 12 Jan 2013; published 28 Jan 2013

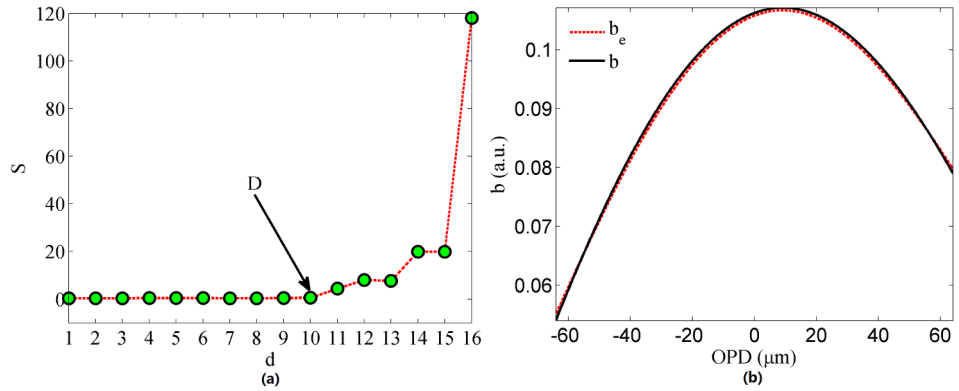

Fig. 3. Background estimation: (a) The absolute value of the summation of the first d IMFS; (b) The assumed background (the solid black curve) and the estimated background (The dotted red curve) obtained from the partial reconstruction with IMFs 11 to 15 and the residual.

3.2 De-noising of the spectrum

3.2.1 De-noising of the polychromatic spectrum

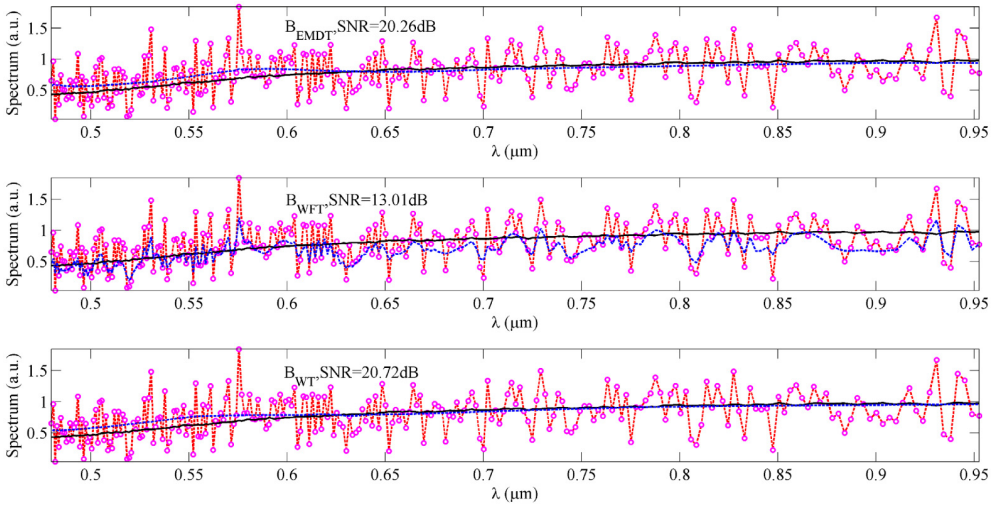

Fig. 4. The de-noised spectrums, whose SNR are 20.26, 13.02 and 20.72 dB, obtained by the EMDT (the upper), WFT (the middle) and WT (the lower) de-noising methods. Herein, the SNR of the contaminated interferogram is 5 dB. The red dashed lines marked with purple circles are the noisy spectrums; the solid black lines are the original noise free spectrums; the dashed blue lines are the de-noised spectrums.

#179604 - $15.00 USD Received 9 Nov 2012; revised 28 Dec 2012; accepted 12 Jan 2013; published 28 Jan 2013

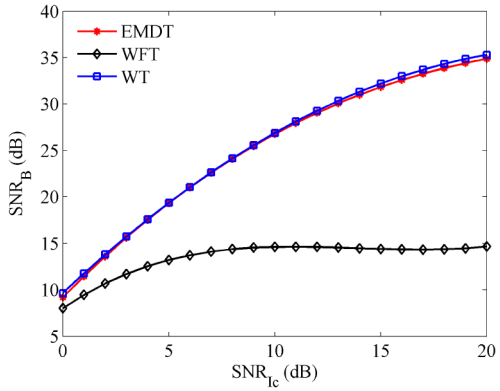

Fig. 5. The SNR of the de-noised spectrums v. s. SNR of the contaminated interferograms.

The interferogram without background was obtained, and the next step is to suppress the effects from the noise during the spectrum reconstruction procedure. Via Fourier transform and the proposed EMD thresholding (EMDT) de-noising method proposed in Sec. 2.2, the noise free spectrums are obtained. Correspondingly, the contaminated spectrum also is de-noised by the wavelet thresholding (WT) and windowed Fourier transform thresholding (WFT) de-noising methods [21,22]. WT de-noising is implemented based on the Symlets 8 wavelet and soft-threshold. The window used in the WFT de-noising method is a Hamming window with the width of 5 pixels. As shown in Fig. 4, the de-noised spectrums obtained by the EMDT, WFT and WT de-noising methods, respectively, are denoted as B_{EMDT}, B_{WFT} and B_{WT}. B_o and B_n are the original noise free and noisy spectrums. It is found that the effects from the noise have been suppressed by the de-noising methods effectively. The SNR of the de-noised spectrums obtained by EMDT WFT and WT de-noising methods are 20.26, 13.02 and 20.72 dB.

In order to evaluate the efficiencies of the methods, we have simulated the de-noising of the noisy spectrums obtained from the interferograms with different noise levels. The simulation result is shown in Fig. 5. It is discovered that an approximately equivalent de-noised result was generated via the EMDT and WT de-noising methods. In contrast, the efficiency of the WFT de-noising method is lower.

3.2.2 De-noising of the monochromatic spectrum

Besides the SNR, we are interested in the spectral resolution of the spectrum while de-noising. In order to quantificationally evaluate the spectrum resolution, a monochromatic light, which is Gaussian profile, is applied to the simulation in this section. As shown in Fig. 6, the de-noised spectrums were obtained via the previous three methods through a similar simulation process in Sec. 3.2.1. It was found that the highest SNR and resolution, the lowest peak value of the de-noised spectrums are obtained by the WFT de-noising method.

#179604 - $15.00 USD Received 9 Nov 2012; revised 28 Dec 2012; accepted 12 Jan 2013; published 28 Jan 2013

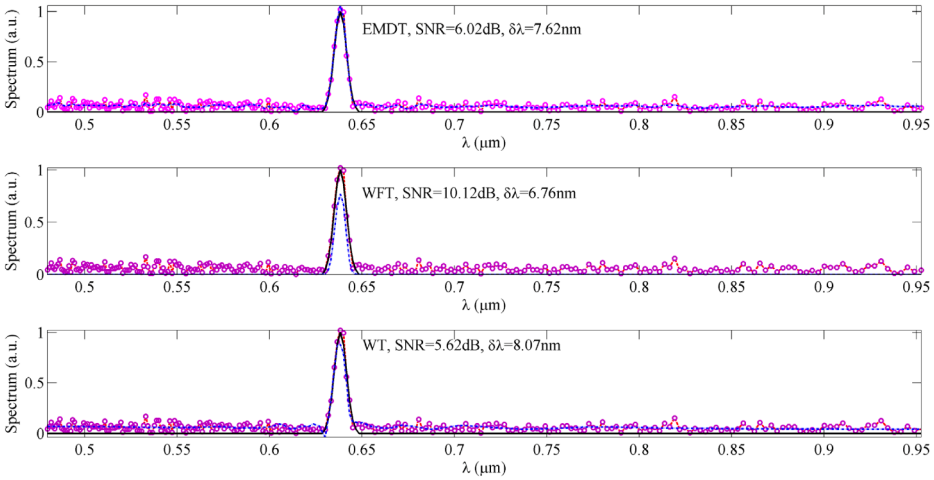

Fig. 6. The de-noised spectrums obtained by the EMDT (the upper), WFT (the middle) and WT (the lower) de-noising methods. $\delta\lambda$ is the spectral resolution of the de-noised spectrum. The SNR and resolution of the de-noised spectrums, respectively, are 6.02, 10.12 and 5.62 dB and 7.62, 6.76 and 8.07nm. Herein, the SNR of the contaminated interferogram is 5 dB. The dashed lines marked with purple circles, solid black lines and dashed blue lines denote the noisy spectrums, the original noise free spectrums and the de-noised spectrums.

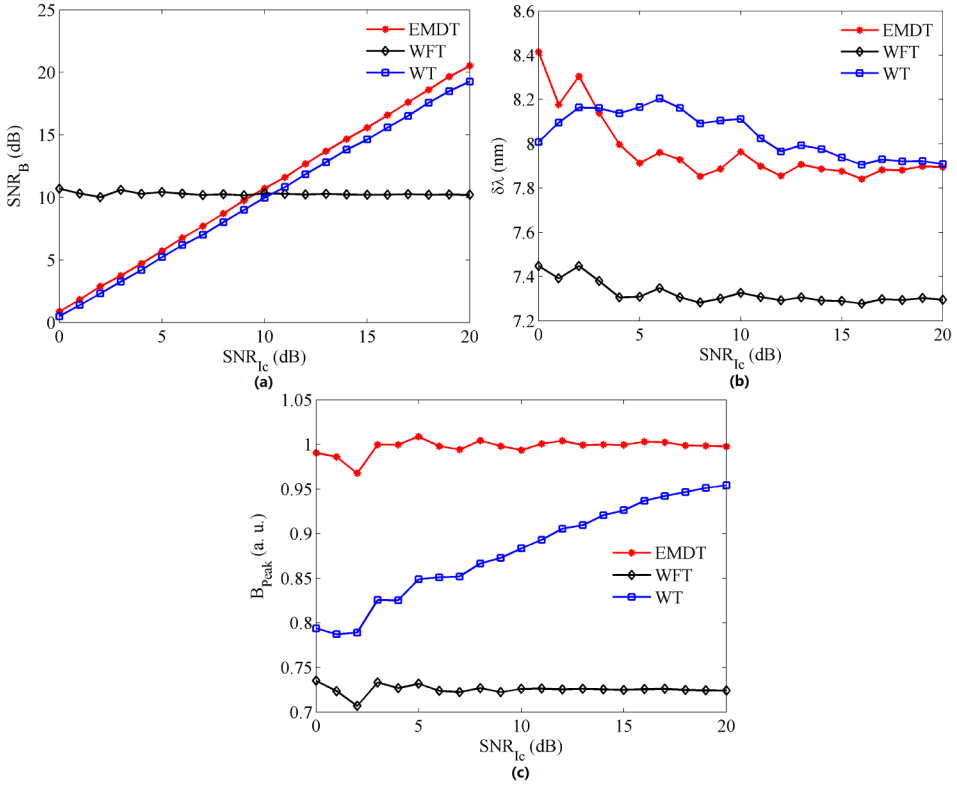

Fig. 7. The de-noising results: The SNR (a), spectral resolution $\delta\lambda$ (b), peak value (c) of the de-noised spectrums B_{Peak} v. s. $\mathrm{SNR}_{\mathrm{Ic}}$.

#179604 - $15.00 USD Received 9 Nov 2012; revised 28 Dec 2012; accepted 12 Jan 2013; published 28 Jan 2013

The result as shown Fig. 6 is obtained while the SNR of the contaminated interferogram is 5 dB. In order to acquire a general conclusion, we have obtained the de-noising results corresponding to different simulated contaminated interferograms with the SNR ranging from 0 to 20 dB. As shown in Fig. 7, the de-noising results are described by the curves of the SNR, spectral resolution and peak value of the de-noised spectrums versus to different SNR of the simulated contaminated interferograms. The SNR of the simulated contaminated interferograms are denoted by SNR_{Ic}. According to Fig. 7, the conclusions can be drawn include: 1) The EMDT de-nosing method is better than the WT de-nosing method; 2) The SNR, spectral resolution and the peak value of the de-noised spectrums obtained by WFT de-noising method are near constant. The near constant variation is introduced by the fixed width of the window function using in WFT. As shown in Fig. 8, the de-noised results are obtained using the WFT methods with different width of the window functions. The peak value decreases with the width of the window. The maximal SNR is obtained while the width of the window is 10. The width of the simulated monochromatic spectrum is also 10. That is, the maximal SNR is obtained while the width of the window is equal to that of the spectrum. The spectral resolution decreases with the width of the window.

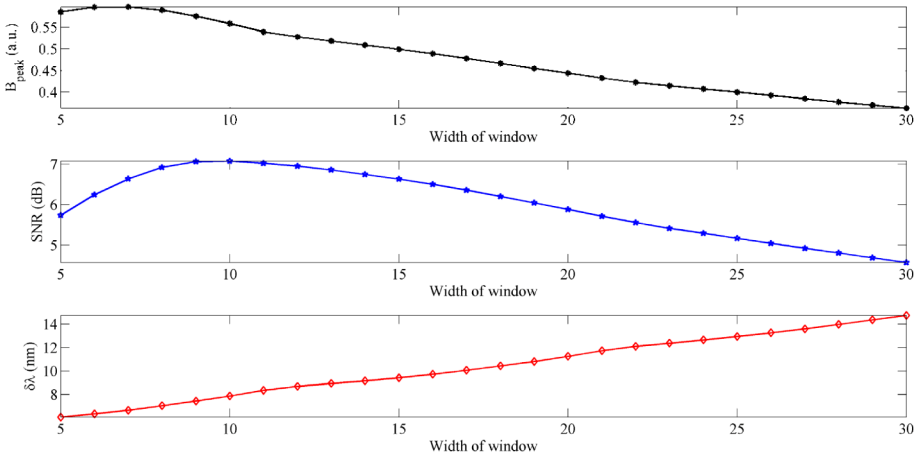

Fig. 8. The de-noised results obtained via the WFT de-noising method with different width of Hamming window functions

#179604 - $15.00 USD Received 9 Nov 2012; revised 28 Dec 2012; accepted 12 Jan 2013; published 28 Jan 2013

3. 2. 3 De-noising of the spectrum from the interferogram contaminated with Poisson noise

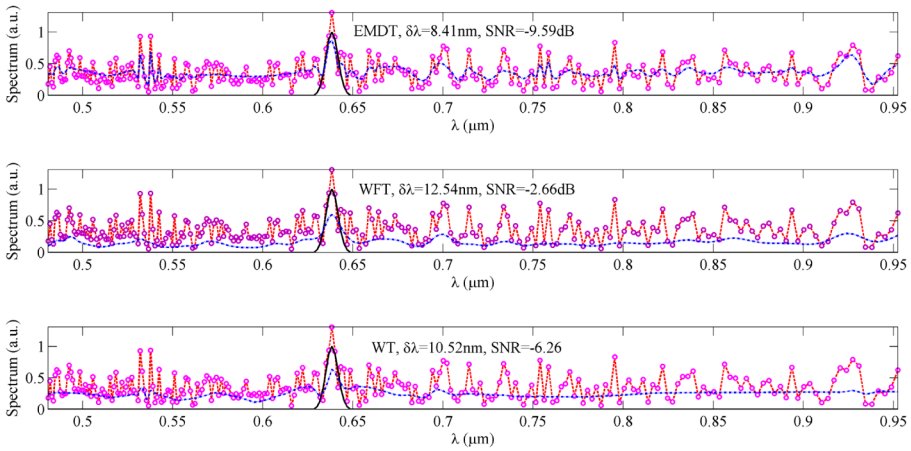

Fig. 9. The de-noised spectrums obtained by the EMDT (the upper), WFT (the middle) and WT (the lower) de-noising methods. $\delta\lambda$ is the spectral resolution of the de-noised spectrum. The SNR and resolution of the de-noised spectrums, respectively, are −9.59, −2.66 and −6.26 dB and 8.41, 12.54 and 10.52nm.The dashed lines marked with purple circles, solid black lines and dashed blue lines denote the noisy spectrums, the original noise free spectrums and the de-noised spectrums.

As shown in Fig. 9, the de-noised spectrums are obtained by the EMDT, WFT and WT de-noising methods. The noisy spectrum is obtained from the interferogram contaminated with the Poisson noise. It can be discovered that the effects from the noise can be suppressed by the EMDT, WFT and WT de-noising methods. However, the result is not as good as the result obtained while the noise is Gaussian noise.

4. Discussion

4.1 Discussions on the assumption in EMDT de-noising method

The EMDT de-noising method is developed based on the assumption that the noise mainly exits in the first IMF of the contaminated spectrum. In order to verify the feasibility of the assumption, we obtained the SNR curves of the spectrums obtained by the proposed methods when we de-noised on the 1st through 5th modes as shown in Fig. 10. The SNR is the maximal when the de-noising is just performed on the first IMFs. That is, the assumption is rational.

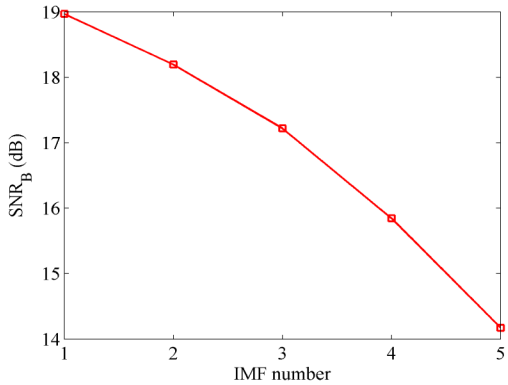

Fig. 10. The de-noising results with respective to the different noise assumptions.

#179604 - $15.00 USD Received 9 Nov 2012; revised 28 Dec 2012; accepted 12 Jan 2013; published 28 Jan 2013

4. 2 Discussions on threshold of in the de-noising methods

As shown in Eqs. (10), the de-noising result is determined by the threshold γ. Therefore, the optimal values of γ in the methods two and three must be ascertained. As shown in Fig. 11, the SNR curves of the noise free spectrums obtained by the EMDT, WFT and WT de-noising methods with different values of γ. It is discovered that the SNR of the de-noised spectrums obtained with the WFT and WT de-noising methods increase and decrease with γ while $\gamma < 0.3$ and $\gamma > 0.3$, respectively. It can be described as that the useful information of the signal is removed while $\gamma > 0.3$. For the EMDT de-noising method, the SNR of the de-noised spectrums increase with γ while $\gamma < 0.5$. The SNR is constant while $\gamma > 0.5$. This phenomenon can be described as that the first IMF of the noisy spectrum has been removed completely while $\gamma > 0.5$.

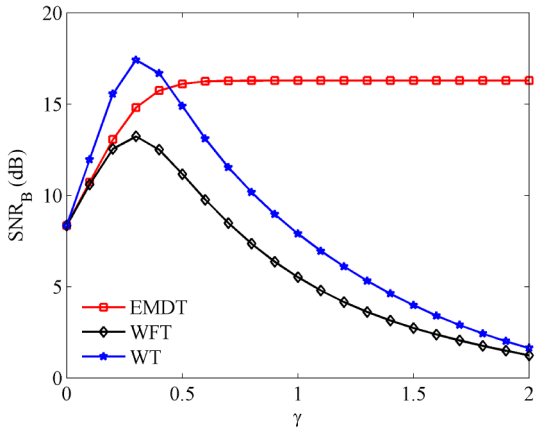

Fig. 11. The de-noising results with respective to the different values of γ.

4. 3 Discussions on the WFT de-noising methods

In Sec. 3.2.1, we have obtained the de-noised result of the polychromatic light using the WFT de-noising method, and the width of the window is 5. Herein, we have obtained the de-noised result using WFT de-noising method with different width of window and threshold. The result is described as the surface as shown in Fig. 12. It can be discovered that the SNR is mainly affected by the threshold.

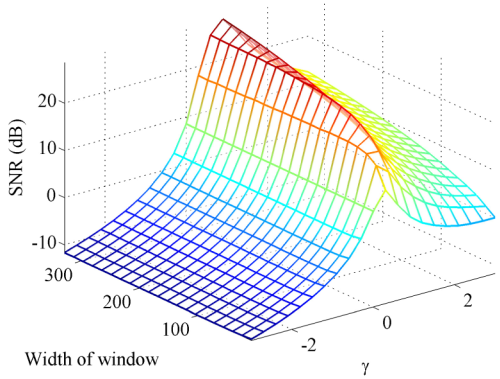

Fig. 12. The SNR of the de-noised polychromatic spectrums obtained by the WFT de-noising method with different width of windows and thresholds.

#179604 - $15.00 USD Received 9 Nov 2012; revised 28 Dec 2012; accepted 12 Jan 2013; published 28 Jan 2013

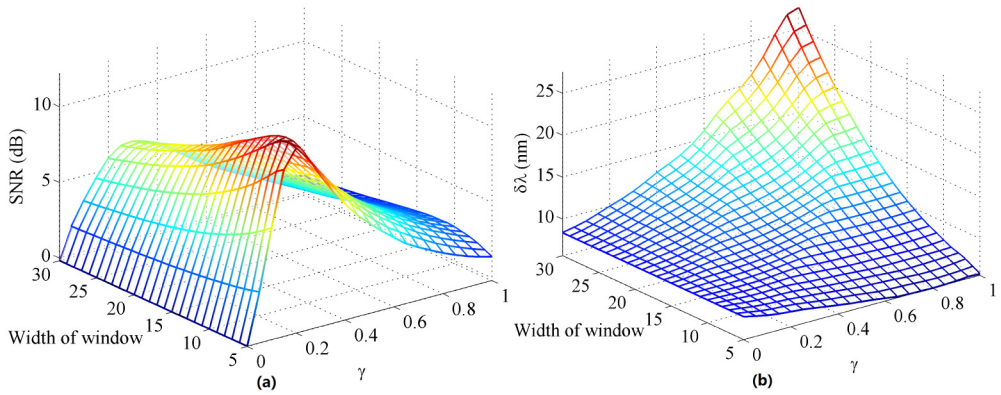

Fig. 13. The SNR (a) and spectral resolution (b) of the de-noised polychromatic spectrums obtained by the WFT de-noising method with different width of windows and thresholds.

Similarly, we have obtained the de-noised result of the polychromatic light. The result is described as Fig. 13. As shown in Fig. 13, the SNR varies with the width of window slightly and with threshold significantly. It is coincident with the de-noised result of the polychromatic light. The spectral resolution is affected by the width of window and threshold significantly. The spectral resolution of the de-noised spectrum is obtained while the width of window is 5.

5. Experimental results

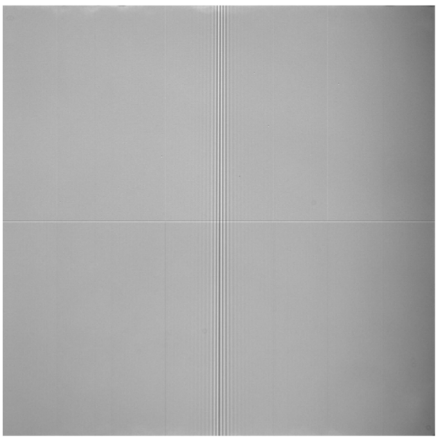

Fig. 14. The measured interferogram.

#179604 - $15.00 USD Received 9 Nov 2012; revised 28 Dec 2012; accepted 12 Jan 2013; published 28 Jan 2013

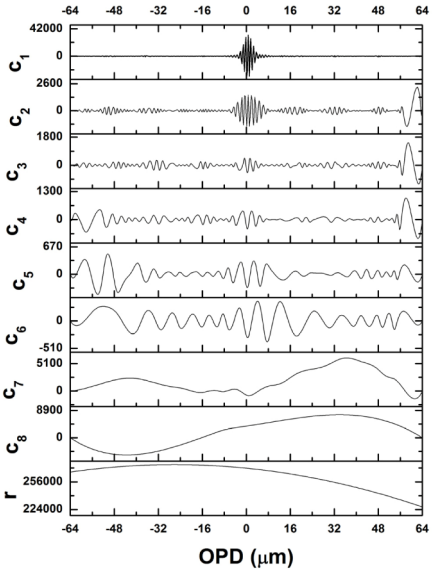

Fig. 15. The measured interferogram is decomposed into 9 IMFs (including the residual mode).

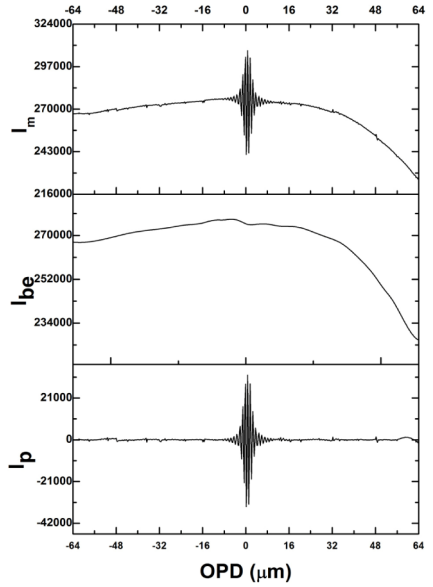

Fig. 16. One row of the measured interferogram I_m, estimated background I_{be} and interferogram without background I_p.

Figure 14 shows the measured interferogram obtained by the PIIS. Based on EMD method, one row measured interferogram, denoted as I_m, is decomposed into 9 IMFs (including the residual) as shown in Fig. 15. The corresponding index D is 6. Therefore, the summation of the 7th and 8th IMFs and residual is regarded as the background. The summation of the 1st through 6th IMFs is regarded as the interferogram without background, I_p. As shown in Fig. 16, the background is almost removed.

#179604 - $15.00 USD Received 9 Nov 2012; revised 28 Dec 2012; accepted 12 Jan 2013; published 28 Jan 2013

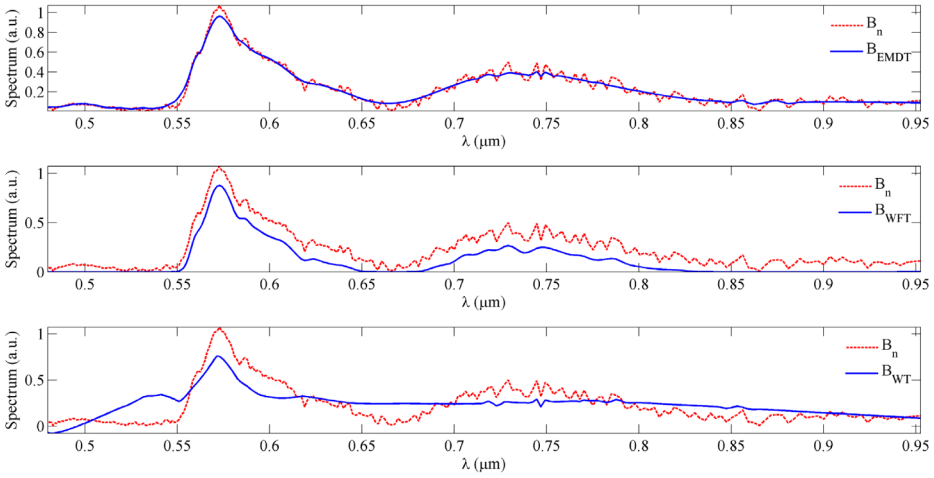

Fig. 17. The noise free spectrum obtained by the proposed methods.

Figure 17 shows the noise free spectrums obtained by the EMDT, WFT and WT de-noising methods. B_n is the noisy spectrum. The fluctuation of the spectrum is suppressed by de-noising effectively. Many other interferograms are processed to verify the robustness of the proposed de-noising methods. It is discovered that the proposed methods are robust.

6. Conclusion

EMD is an excellent tool for analyzing non-stationary and nonlinear data, and can easily be applied to process the data taken by the PIIS. Based on EMD, the methods have been proposed to remove the background of interferogram and to suppress the effects introduced by the noise of spectrum. According to the simulation, it is discovered that the proposed methods are effective. The assumption of the noise mostly exists in the first IMF of the spectrum is feasible. Comparing the EMDT with WFT and WT de-noising methods, it was found that the EMDT de-noising method is effective. In addition, the methods have been used to suppress the effect from the Gaussian and Poisson noise. It was found that the methods are more effective to suppress the effects from the Gaussian noise. The further work is to improve the de-noising method for the Poisson noise. The data measured by the PIIS was also processed by the proposed methods for the background removal and de-noising. In conclusion, the EMD is adaptive and robust for the removal of the background and the suppression of the effects introduced by the noise.

Acknowledgments

This work was supported by the 863 Program (2012AA121101), the major state special project (E0310/1112/JC02) and the National Natural Science Foundation (61275184).

#179604 - $15.00 USD Received 9 Nov 2012; revised 28 Dec 2012; accepted 12 Jan 2013; published 28 Jan 2013